Sridhav Krishnaswamy
Research Fellow.

Ares J. Rosakis
Assoc. Professor,
Assoc. Mem. ASME

Graduate Aeronautical Laboratories,
California Institute of Technology,
Pasadena, CA 91125

G. Ravichandran
Asst. Professor,
University of California,
San Diego, CA
Assoc. Mem. ASME

On the Extent of Dominance of Asymptotic Elastodynamic Crack-Tip Fields: Part II—Numerical Investigation of Three-Dimensional and Transient Effects

In Part I of this paper, the question of the extent of dominance of the mode I asymptotic elastodynamic crack-tip field (the K_I^d*-field) was studied experimentally. Here, the results of two and three-dimensional elastodynamic finite element simulations of the drop-weight experiments are reported. The load records as obtained from the impact hammer and supports of the drop-weight loading device were used as boundary tractions in the numerical simulations. For the laboratory specimen studied, the results of the simulations indicate that the asymptotic elastodynamic field is not an adequate description of the actual fields prevailing over any sizeable region around the crack tip. This confirms the experimental results of Part I which showed that three-dimensional and transient effects necessarily have to be taken into account for valid interpretation of experimental results.*

1 Introduction

It is increasingly being recognized that the stress and displacement fields near the tip of a crack are essentially three-dimensional in nature. Exact analytical solutions for the three-dimensional crack problem, however, do not exist in general. Thus, finite elements have been used extensively to gain an understanding of the three-dimensional structure of the crack-tip fields. For example, Levy, Marcal, and Rice (1971), Parsons, Hall, and Rosakis (1986), and Nakamura and Parks (1987) have investigated three-dimensional crack problems under elastostatic conditions. In addition, Narasimhan and Rosakis (1988) and Nakamura and Parks (1988) have recently studied the three-dimensional elastoplastic state prevailing near the tip of a static crack.

The finite element method has also been used to study three-dimensional dynamic fracture problems. For the most part, however, special singular elements have been used to model the crack tip. The purpose of employing singular elements has been to *bias* the near-tip field to have a particular (asymptotically known) structure in order to extract the magnitude of crack-tip singularities (the stress intensity factor, J-integral, etc). For instance, Nakamura, Shih, and Freund (1986) have analyzed the three-point bend configuration under idealized dynamic loading conditions. Their primary objective was to identify conditions under which experimentally obtained quantities could be used to directly infer the initiation value of the J-integral under elastoplastic conditions.

Smith and Freund (1988) were the first to investigate in detail the nature of the near-tip three-dimensional elastic fields for a steady-state, dynamically propagating crack under Mode I conditions. They, however, *imposed* the plane-stress dynamic stress intensity factor field (the K_I^d-field) as the far-field boundary condition. As pointed out in Part I of this paper, one of the most important pieces of information that the experimentalist would like to have is the extent to which the K_I^d-field models the near-tip stresses and displacements. Most of the experimental results reported in the literature rely on the assumption of K_I^d-dominance around the crack tip. The adequacy of such an assumption therefore needs to be studied.

In Part I, the issue of K_I^d-dominance was studied through a series of drop-weight experiments in conjunction with the method of *bifocal caustics*. The results of the experiments indicated that the assumption of K_I^d-dominance could lead to substantial errors in the measured results. In this paper, the finite element method is used to investigate this issue further. No attempt is made to bias the near-tip singularity; nor is the far-field boundary condition constrained to be given by the plane-stress asymptotic field.

Contributed by the Applied Mechanics Division of The American Society of Mechanical Engineers for publication in the Journal of Applied Mechanics.

Discussion on this paper should be addressed to the Technical Editor, Prof. Leon M. Keer, The Technological Institute, Northwestern University, Evanston, IL 60208, and will be accepted until two months after final publication of the paper itself in the Journal of Applied Mechanics. Manuscript received by the ASME Applied Mechanics Division, Mar. 31, 1989; final revision, Mar. 14, 1990.

A series of two and three-dimensional finite element simulations[1] of the drop-weight experiments (reported in Part I) were done using the experimentally recorded impact and support-point load histories as boundary tractions for the simulations. The simulations were undertaken in an effort to qualitatively capture the essential features of the experimental results. Only the case of the dynamically loaded stationary crack was considered for the simulations. It was felt that attempting to simulate the case of a propagating crack would be premature at this point, especially since it entails a high degree of uncertainty in terms of the nodal-release procedure that would have to be used. The primary interest here is in trying to identify the role of specimen geometry, dynamic loading, and the three-dimensional structure of the crack-tip region (especially under transient conditions) insofar as these have a bearing on the K_I^d-dominance assumption on which the experimental methods rest.

Three issues are addressed. First, where relevant, direct comparisons of the numerical results with the corresponding asymptotic field are made to ascertain the adequacy of the K_I^d-field as a characterizer of the near-tip continuum fields. All field quantities presented are normalized in such a manner as to highlight salient points. Thus, full-field two-dimensional results are compared with the asymptotic field and three-dimensional results are normalized by the appropriate two-dimensional or asymptotic values. Secondly, virtual energy release rate integrals evaluated numerically are used to extract stress intensity factor values in order to compare with the experimentally measured values. Finally, the implications of the finite element results are studied with regard to the experimental method of caustics in reflection. In an attempt to qualitatively recover the results of the drop-weight experiments, an exact analog of the procedure used in the experiments is attempted in the following manner. As explained in Part I, the out-of-plane surface displacement fields obtained from the analyses are used to numerically generate (synthetic) caustic patterns for a range of initial curves. That is, the numerically obtained surface out-of-plane displacement field u_3 $(x_1, x_2, h/2)$ is subjected to the optical mapping

$$\mathbf{X} = \mathbf{x} + 2z_0 \nabla u_3(x_1, x_2, h/2) \quad (1)$$

for a set of values for parameter z_0 (the object plane distance). Here, $\mathbf{x}$ are points on the specimen that are optically mapped onto points $\mathbf{X}$ on the object plane, and h is the specimen thickness. These caustics are then interpreted exactly as in the experiments; i.e., the caustic diameters are related to the stress intensity factor under the assumption that the underlying out-of-plane displacement field is K_I^d-dominant. Thus, the transverse diameters of the synthetic caustics are used to extract the apparent stress intensity factor values through the relation

$$K_I^d = \frac{ED^{5/2}}{z_0 \nu h} f(\dot{a}, \nu), \quad (2)$$

where D is the transverse diameter of the caustic, ν is Poisson's ratio and E is the Young's modulus of the material, h is the specimen thickness, $\dot{a}$ is the crack velocity, and f is a known function of crack velocity and material properties (see Part I for details). Again, as in the experiments, if the displacement field is not actually K_I^d-dominant, this fact would be reflected as an apparent (erroneous) dependence of the stress intensity factor on the radial distance from the crack front.

It must be pointed out that in the ensuing discussion of two-dimensional results, all in-plane lengths are normalized by the (actual) specimen thickness, h. For a two-dimensional problem, however, the plate thickness is not a relevant length scale. This is done here purely for ease of reference with subsequent three-dimensional results.

2 Two-Dimensional Elastodynamic Simulations

The simulations of the dynamic experiments were first attempted under the simplifying assumption that the specimens could be considered to be essentially under plane-stress conditions. Before delving into the simulations of the experiments, one issue needs to be addressed. Since no special singular elements were used in the finite element analyses, it is essential that the discretization used must be such as to capture the expected singular crack-tip fields adequately. To this effect, preliminary two-dimensional elastostatic analyses of the three-point bend specimen were performed. Based on the results of these, the mesh discretization shown in Fig. 1 consisting of 396 isoparametric linear quadrilateral elements (425 nodes) was found to be adequate. This mesh has a focused region around the crack-tip of about one (actual) specimen thickness which is divided into 18 sectors and 10 concentric rings of elements. The crack-tip elements are four-noded quadrilaterals collapsed into triangles. The mesh discretization was found to adequately capture the square-root singular field near the crack tip for the elastostatic case and was thus deemed suitable for the dynamic problem as well.

For the two-dimensional elastodynamic simulations, the loads as obtained from the experimental tup records (Fig. 2) were applied as the boundary conditions. That is, the impact-tup load history was applied to the nodes corresponding to the impact tup, and the support-tup load history was applied to the associated nodes as shown in Fig. 1. From symmetry conditions, the uncracked ligament was constrained to move only along the x_1-direction. The rest of the boundary was left free

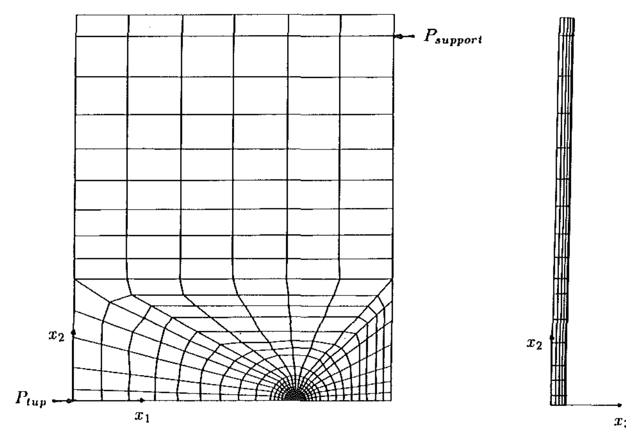

Fig. 1 Mesh geometry

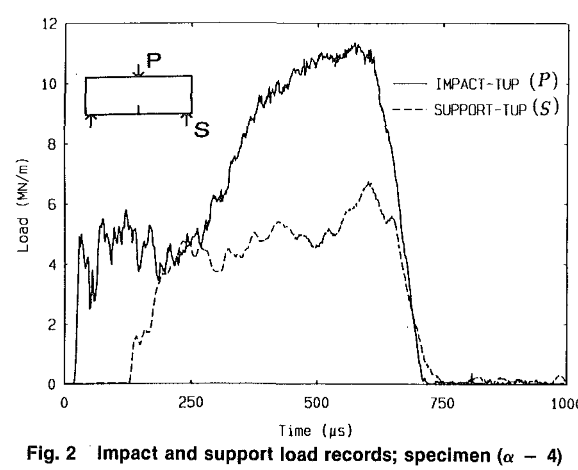

Fig. 2 Impact and support load records; specimen (α – 4)

[1] All the numerical computations were done using a much modified version of the finite element analysis program FEAP whose ancestry traces back to Taylor (1977).

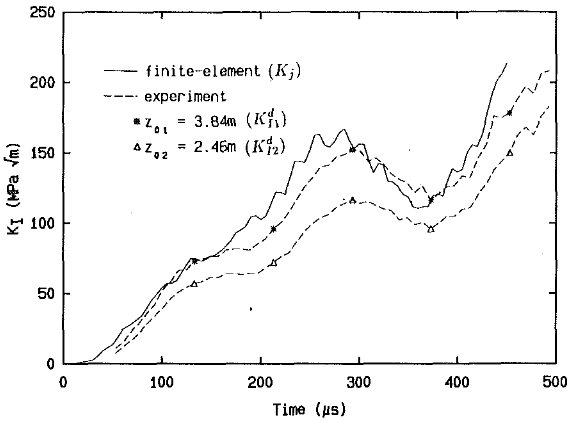

Fig. 3(*a*) Comparison of experimentally obtained dynamic stress intensity factor history with that computed from a two-dimensional simulation; specimen (v 3s)

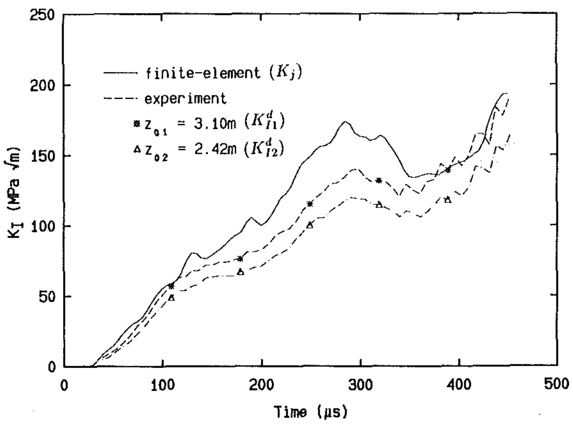

Fig. 3(*b*) Comparison of experimentally obtained dynamic stress intensity factor history with that computed from a two-dimensional simulation; specimen (α − 4)

of traction. An implicit Newmark predictor-corrector time integration scheme (see Hughes and Belytschko, 1983) was used for its virtue of unconditional stability which would allow for relatively large time steps and the attendant loss of high-frequency information was deemed acceptable since it is not the intent here to monitor discrete stress waves in the body. The time steps chosen for the numerical integration were thus based only on accuracy considerations.

The (virtual) energy release rate for a dynamically loaded stationary crack is given by (see Nakamura, Shih, and Freund, 1986)

$$J=\lim_{\Gamma\to 0}\int_\Gamma\left((U+T)n_1-\sigma_{ij}n_j\frac{\partial u_i}{\partial x_1}\right)d\Gamma, \tag{3}$$

where U is the strain energy density, T is the kinetic energy density, σ_{ij} is the stress tensor, $\mathbf{u}$ is the displacement vector, and $\mathbf{n}$ is the unit outward normal to the contour of integration Γ. Here, $\Gamma \to 0$ symbolically indicates that the integration contour must be shrunk on to the crack tip. In the simulations, the time history of this integral was computed using the equivalent domain integral form described in Nakamura, Shih, and Freund (1986). The dynamic stress intensity factor was then computed through the relation between K_I^d and J in plane stress,

$$K_I^d = \sqrt{EJ}, \tag{4}$$

where E is the Young's modulus of the material. Figures (3*a*), (3*b*) show the experimentally obtained dynamic stress intensity factor history in comparison with that from the numerical simulations for specimens ($v3s$) and ($\alpha-4$). Here, K_{I1}^d and K_{I2}^d

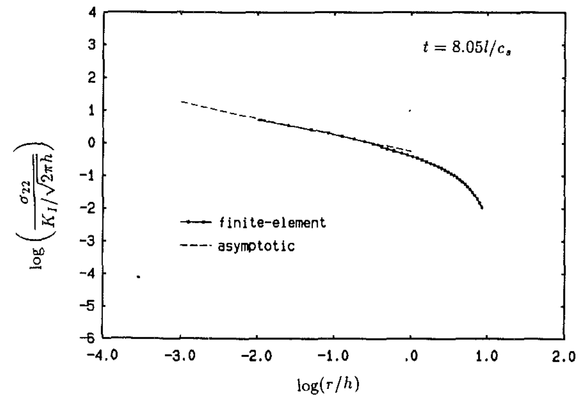

Fig. 4 Plot of log ($\sigma_{22}\sqrt{2\pi h}/KK_I^d(t)$) versus log ($r/h$) for the two-dimensional elastodynamic case

refer to the experimentally measured values corresponding to the two object plane distances z_{01} and z_{02} (see Part I for details) and K_J is that computed from the dynamic simulations (through the J-integral). It is seen that in both cases K_J has the same general trend as K_{I1} and K_{I2} except that the experimental values are sometimes substantially lower, while at other times equal to or higher than the simulated values. This discrepancy is attributable to two sources. First, there are uncertainties associated with the simulations in terms of how accurately the tup records provide the boundary tractions actually experienced by the specimens. Secondly, and more importantly, there is the possibility that the experimental values might not have been obtained from a region of K_I^d-dominance. This is in fact foreshadowed by the discrepancy between the two experimental records themselves.

In the above, it has been implicitly assumed that the asymptotic K_I^d-field has validity for this (two-dimensional) geometry and dynamic loading condition. However, as pointed out in Part I, the existence of a stress intensity factor field around a dynamically loaded stationary crack in a finite geometry has not been universally established. It is thus necessary to check whether a square-root singular asymptotic field is appropriate here. To this end, a logarithmic plot of stress component σ_{22} along the $\theta = 5$ deg line versus the logarithm of radial distance from the crack tip is shown in Fig. 4 for one representative time in the simulation. Comparison with the corresponding curves for the asymptotic field (with the values of the stress intensity factor obtained from the J-integral) indicates that a square-root singular field is indeed asymptotically descriptive of the near-tip continuum structure for this two-dimensional configuration at least for the times shown.

As a measure of the extent of dominance of the asymptotic K_I^d-field, the angular variation of the stresses and displacements for a range of radial distance is shown in Figs. 5(*a*), 5(*b*) for one particular time. Also shown for comparison are the corresponding asymptotic values. Note that the normalization used here is such that the asymptotic values are given by a single curve for *any* radial distance. This normalization enables distinct features of the stress intensity factor field to be discerned in the near-tip full-field solution. The magnitudes, however, are seen to vary with increasing radial distance from the crack tip.

A quantity of fundamental interest for the method of caustics in reflection is the out-of-plane displacement field, u_3. The plane-stress condition that $\sigma_{33} = 0$ provides the following relation for the out-of-plane displacement field:

$$u_3 = -\frac{\nu h}{2E}(\sigma_{11}+\sigma_{22}), \tag{5}$$

where h is the actual specimen thickness. The angular variation of this is shown in Fig. 6 for two radial distances from the

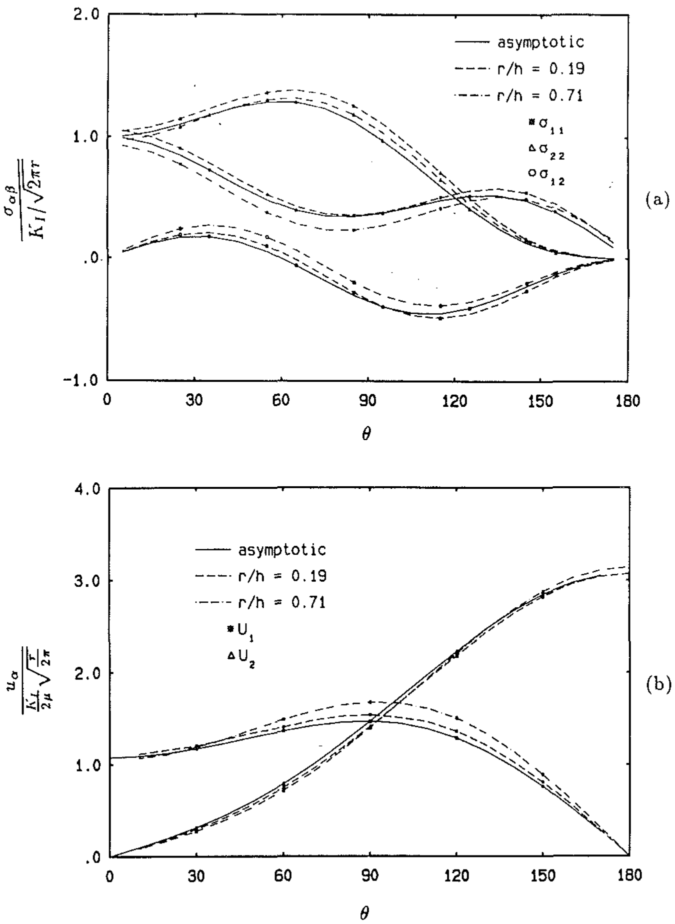

Fig. 5 Angular variation of near-tip (a) stresses and (b) in-plane displacements for the two-dimensional case in comparison with the corresponding asymptotic values

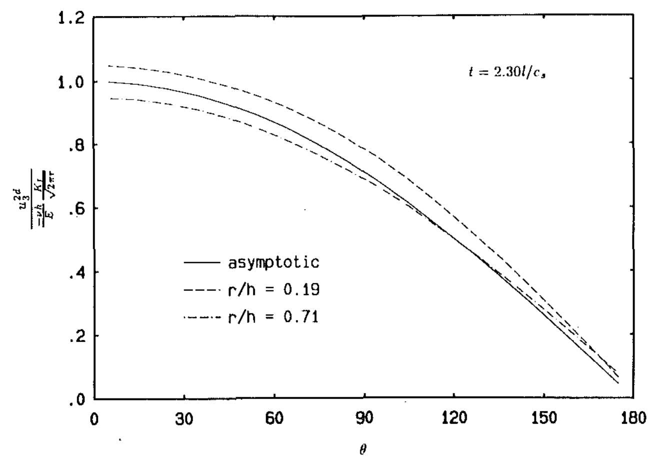

Fig. 6 Angular variation of computed out-of-plane displacements for the two-dimensional case in comparison with the corresponding asymptotic values

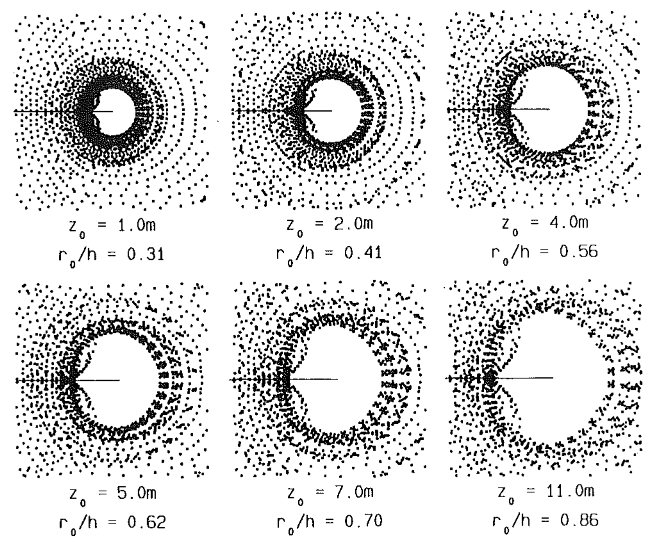

Fig. 7(a) Numerically generated caustics from the two-dimensional elastodynamic simulation

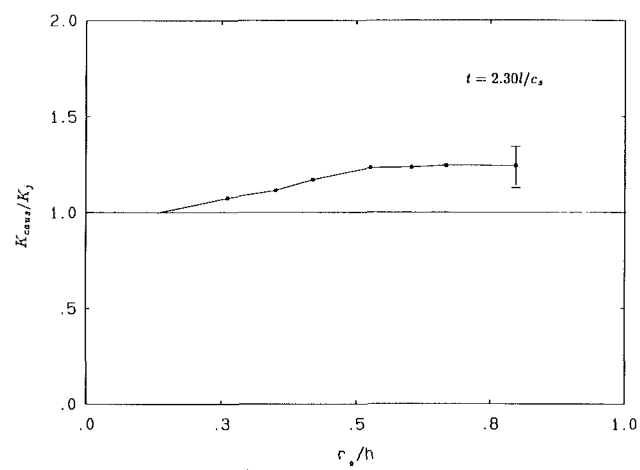

Fig. 7(b) Plot of K_{caus}/K_J versus r_0/h from the two-dimensional elastodynamic simulation

crack tip. Again, u_3 is normalized by the corresponding asymptotic quantity. It can be seen that the full-field quantity is in reasonable qualitative agreement with the asymptotic expression for $r/h \to 0$ with increasing deviation in magnitude as r/h increases. This was seen to be the case for other times in the simulation as well. Note, again, that normalization of two-dimensional results with respect to the (actual) specimen thickness is done purely for comparison purposes with subsequent three-dimensional results.

Finally, synthetic caustics were obtained from the out-of-plane displacement field for various times in the simulation. Since linear finite elements were used and, in plane-stress problems, the out-of-plane displacement field is obtained from the in-plane stress field, a smoothing scheme given in Hinton and Campbell (1974) was used to obtain the derivatives of the surface-displacement field required in the caustic mapping of the surface. A representative set of these caustic patterns is shown in Fig. 7(a) for one particular time in the simulation and for a set of z_0s. The corresponding initial-curve radii computed on the basis of the caustic diameters (see Part I for details) range from r_0/h of 0.31 to 0.86. These caustics are seen to have the epicycloidal shape characteristic of those from the asymptotic solution. The ratio of the stress intensity factor computed from the diameters of these synthetic caustics (denoted K_{caus}) to that obtained from the J-integral (K_J) are plotted in Fig. 7(b) as a function of the initial curve radius of the numerical caustic. While the apparent measured stress intensity factor seems to increase as r_0/h increases, to within the accuracy warranted by the procedure used here, it appears that caustics should provide the stress intensity factor value (to within 20 percent) for initial curve radii in the range $r_0/h \leq 0.8$. Even though this error is substantial, it is clear that two-dimensional transient effects alone would not seem to entirely account for the much larger variation in the stress intensity factor observed in the experiments. Indeed, it is worth noting that the above result would indicate that caustics should always overestimate K_j which is not necessarily the case in the experiments (see Figs. 3(*a*), 3(*b*)).

3 Three-Dimensional Elastodynamic Simulation

It appears that the substantial variation observed between the experimentally measured stress intensity factors from bifocal caustics (see Part I) cannot be explained purely in terms of (two-dimensional) dynamic effects affecting the caustic patterns. Thus, additional reasons must be sought in terms of (a) nonlinear effects or (b) three-dimensional effects under transient conditions. Visual evidence of the plastic deformation in the fractured specimens indicated that the initial curves for the experimental caustics were well outside the plastic zone whose *maximum extent* was seen to be confined to $r_p/h \leq 0.15$ (Krishnaswamy, 1988). Based on the estimates of Rosakis and Freund (1981), the experimental results of Zehnder and Rosakis (1988), as well as elastoplastic simulations of the current experiments, plasticity effects were found to be minimal. Thus, attention will now be directed toward studying the effect of three-dimensionality near the crack tip by means of a full-field three-dimensional elastodynamic simulation of the drop-weight experiments.

The mesh geometry used had an in-plane layout identical to that used for the two-dimensional cases (Fig. 1). This enables direct comparison of three-dimensional results with the corresponding plane-stress simulations and thereby helps identify the effect of three-dimensionality. Five layers of 8-noded brick elements through half the thickness leading to a total of 1960 elements (2550 nodes) were used to model one-quarter of the three-dimensional body. The crack-tip elements were collapsed to form triangular wedges. Recognizing that the largest through-thickness variations in field quantities occur near the free surface, the mesh was graded in the thickness direction such that the layer interfaces were at $x_3/h=0$, 0.15, 0.275, 0.375, 0.45, and 0.5. The experimentally obtained tup load histories interpreted as uniform line loads through the thickness were applied as boundary conditions to the appropriate nodes. The uncracked ligament surface and the specimen midplane were constrained suitably as dictated by symmetry considerations. The rest of the boundary was left traction-free. Once again, an implicit Newmark predictor-corrector scheme was used in order to be consistent with the algorithm used for the two-dimensional simulation.

Following Nakamura, Shih, and Freund (1986), an average dynamic energy release rate integral appropriate for the three-dimensional case can be defined as:

$$J_{av}=\frac{1}{h}\lim_{S\to 0}\int_S\left((U+T)n_1-\sigma_{ij}n_j\frac{\partial u_i}{\partial x_1}\right)dS, \tag{6}$$

where S is now a tubular surface through the specimen and $S\to 0$ symbolically indicates that this surface is shrunk onto the crack front. In order to compare with experimental results, an "average" stress intensity factor is extracted from J_{av} through relation (4). The average energy release rate value obtained from the three-dimensional simulation is shown in Fig. 8 and is seen to be not much different from that computed in the plane-stress analysis. This suggests that the plane-stress approximation might be adequate if one is merely interested in integrated energy release rate type of quantities.

From the point of view of the method of caustics in reflection, the primary issue is the extent of deviation of the near-tip surface out-of-plane displacement field from the corresponding asymptotic plane-stress expression. This is shown in Fig. 9(*a*) for a set of radial lines along $\theta = 0$ deg, 60 deg, and 140 deg and for one typical time. The surface u_3-displacements as obtained from the three-dimensional solution are normalized by the corresponding asymptotic values. The two-dimensional counterpart along the radial line $\theta = 0$ deg is shown for comparison purposes. Two salient features can be identified from this figure. First, the *two-dimensional* full-field values seem to be in good agreement with the asymptotic for sufficiently small radial distances. The asymptotic expression becomes increasingly inaccurate for larger radial distances. Secondly, it is precisely in those regions where the two-dimensional and asymptotic fields are in close agreement that the three-dimensional structure deviates the most from the asymptotic. In Fig. 9(*b*), the angular variations of the surface u_3-displacements are shown for a range of r/h. Under the normalization used, the asymptotic u_3-displacement are given by $\cos(\theta/2)$—the solid line—for any radius. Again, it is noted that the asymptotic field does not always model the actual three-dimensional structure very well. Indeed, the deviation from the asymptotic is seen to be pronounced toward the crack tip. For larger r/h, the theta variation of u_3 seems to approach the asymptotic curve in form, though not in actual magnitude. Further, Fig. 9(*c*) clearly brings out the deviation of the actual three-dimensional field from the corresponding asymptotic values. Here, contours of constant free-surface u_3-displacements from the three-dimensional analysis are shown in the top half of the figure. The bottom half shows the *corresponding* contours as if the asymptotic K_I^d-field had prevailed. It appears that the actual three-dimensional field is not quite captured by the asymptotic expression for the surface out-of-plane displacements—toward the crack tip because of substantial three-dimensional effects and away from it because the asymptotic expression becomes increasingly insufficient.

The qualitative effects of the above features insofar as these affect the method of caustics can now be evaluated. As described previously, the three-dimensional surface out-of-plane displacements obtained numerically for various times in the simulation are mapped using equation (1) to obtain synthetic caustic patterns. A representative sequence of these caustic patterns for one particular time is shown in Fig. 10(*a*). These were obtained for the same instant of simulation and for the same set of z_0s as were used in the two-dimensional case. The role of three-dimensionality is thus clearly brought out. The graphic contrast that emerges between the caustic patterns obtained under two-dimensional assumptions and the actual three-dimensional conditions can be seen by comparing Figs. 7(*a*) and 10(*a*). In comparison to the corresponding two-dimensional results, it is noted that for small r_o/h, the shadow spots in Fig. 10(*a*) are less epicycloidal in shape and much smaller in size. This is not surprising considering the angular variations of u_3 which deviated markedly from the asymptotic value as $r/h \to 0$. Compare this with the results of the plane-stress analysis (see Fig. 7(*a*)) where the qualitative agreement with the asymptotic field appears to be much better over a wider range of r/h. If, now, one were to relate the caustic

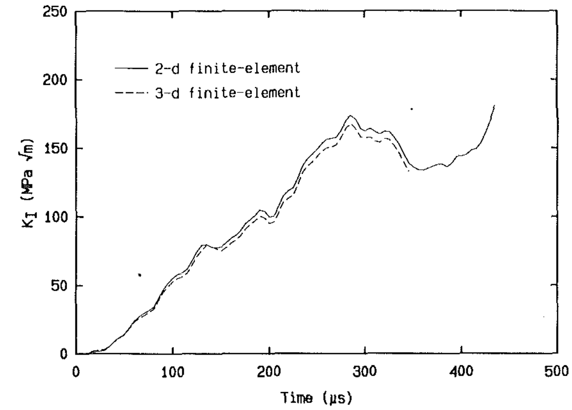

Fig. 8 Comparison of "average" dynamic stress intensity factor history as computed from two and three-dimensional simulations

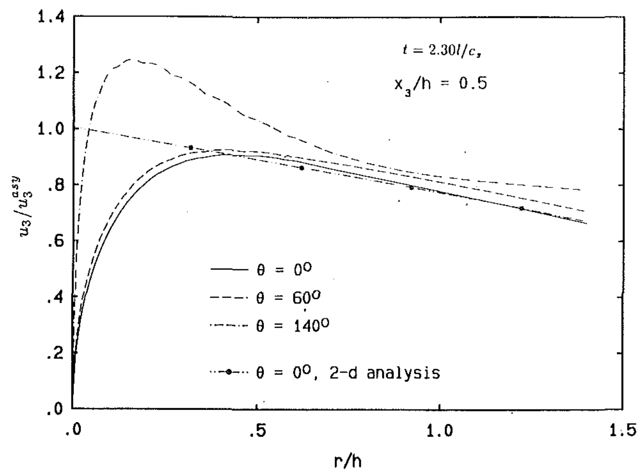

Fig. 9(*a*) Radial variation of the free surface u_3-displacements in comparison with the corresponding asymptotic values

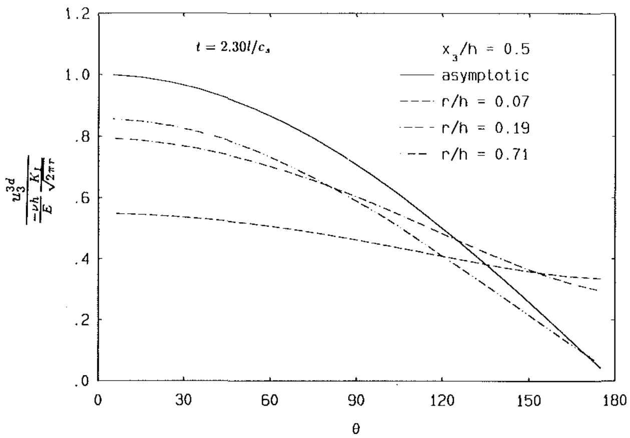

Fig. 9(*b*) Angular variation of the free surface u_3-displacements in comparison with the corresponding asymptotic values

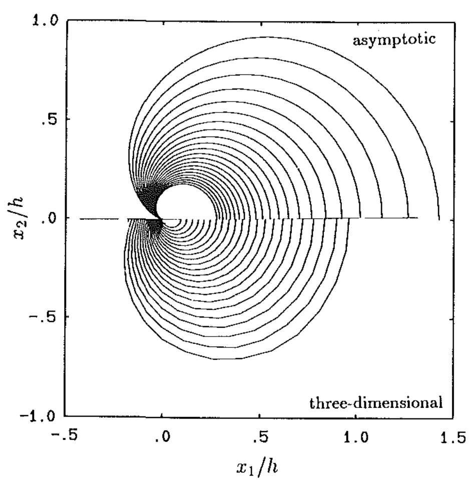

Fig. 9(*c*) Contours of constant free surface u_3-displacements in comparison with the corresponding asymptotic values

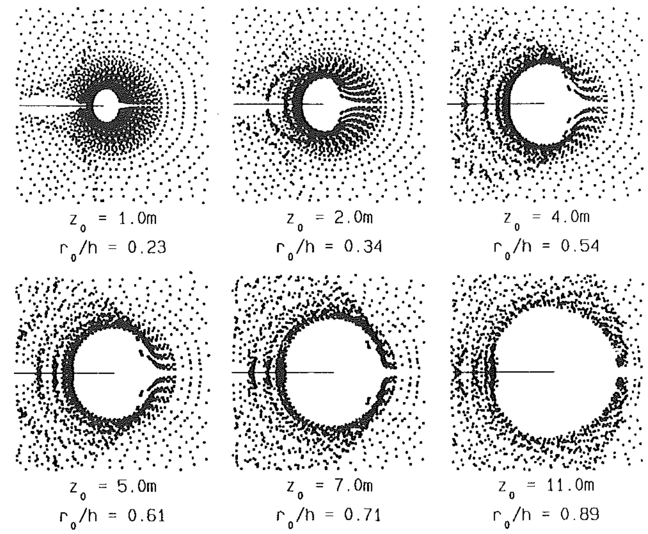

Fig. 10(*a*) Numerically generated caustics from the three-dimensional elastodynamic simulation

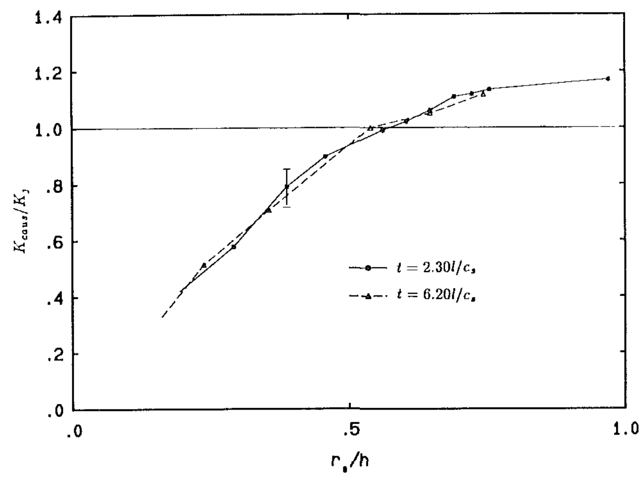

Fig. 10(*b*) Plot of K_{caus}/K_J versus r_0/h from the three-dimensional elastodynamic simulation

diameters to the stress intensity factor through equation (2), then the resulting value of K_{caus}/K_J (shown for two times) is seen to vary quite substantially with increasing initial curve radius as shown in Fig. 10(*b*). From the figure, it is seen that as $r_0/h \rightarrow 0$, the measured stress intensity factor value becomes substantially less than the value obtained from the domain integral. Further, for larger initial curve radii, it is possible for caustics to provide an overestimate of K_J. More importantly, the almost monotonically increasing K_{caus}/K_J versus r_0/h curve for the three-dimensional transient simulation case qualitatively captures essentially all the features observed experimentally. Thus, the apparent dynamic stress intensity factor, as measured by the method of caustics, would seem to increase with increasing initial-curve radii. Also, in view of the lack of a sizeable domain of dominance of the K_I^d-field, it would appear that the agreement between the measured dynamic stress intensity factor history and that computed through the *J*-integral cannot be expected to be any better than obtained in Figs. 3(*a*), 3(*b*).

As a parenthetical note, it is interesting that the variation in K_{I1}^d and K_{I2}^d—the two values for the dynamic stress intensity factor as measured from pairs of bifocal caustics—turns out to be in quite good *quantitative* agreement with the results of Fig. 10(*b*). That is, the ratio of K_{I1}^d to K_{I2}^d as obtained from experiments seem to be in close agreement with that obtained from Fig. 10(*b*) for the corresponding initial curve radii. This can be seen in Fig. 11 where the numerically generated results of Fig. 10(*b*) are used to "scale" the results of one particular experiment. To do this, *assume* that the results of Fig. 10(*b*) (K_{caus}/K_J versus r_0/h) hold for the whole duration of the loading. The experimental data (corresponding to the two z_0s) shown in Fig. 11(*a*) can then be scaled, for each time, to the corre-

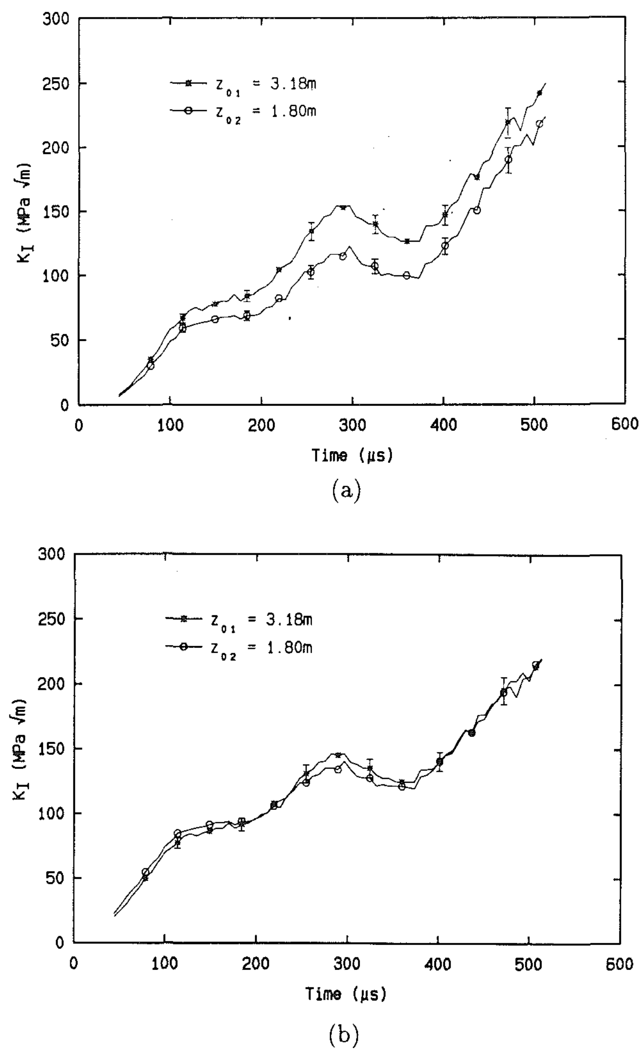

Fig. 11 (*a*) **Raw and** (*b*) **"scaled" experimental data for specimen (3*q*)**

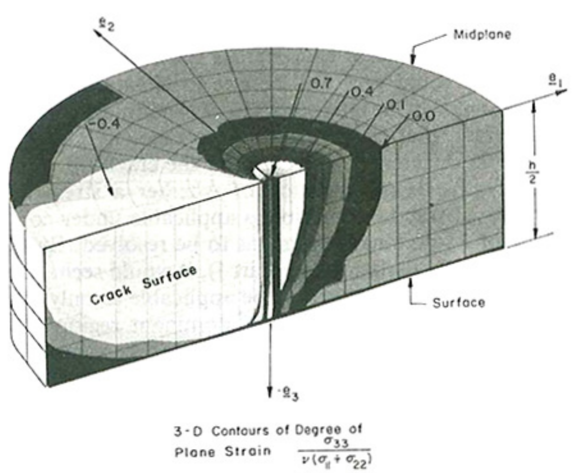

Fig. 12 Representative near-tip variation of the degree of plane strain

sponding "K_j" value by means of Fig. 10(*b*). The resulting "scaled" dynamic stress intensity factor histories corresponding to the two z_0s are shown in Fig. 11(*b*). It is seen that by this procedure the deviation between the K_I^d-values observed in the experiments from pairs of bifocal caustics essentially reduce to within expected experimental scatter for the whole duration of loading. Thus, it would appear that the main

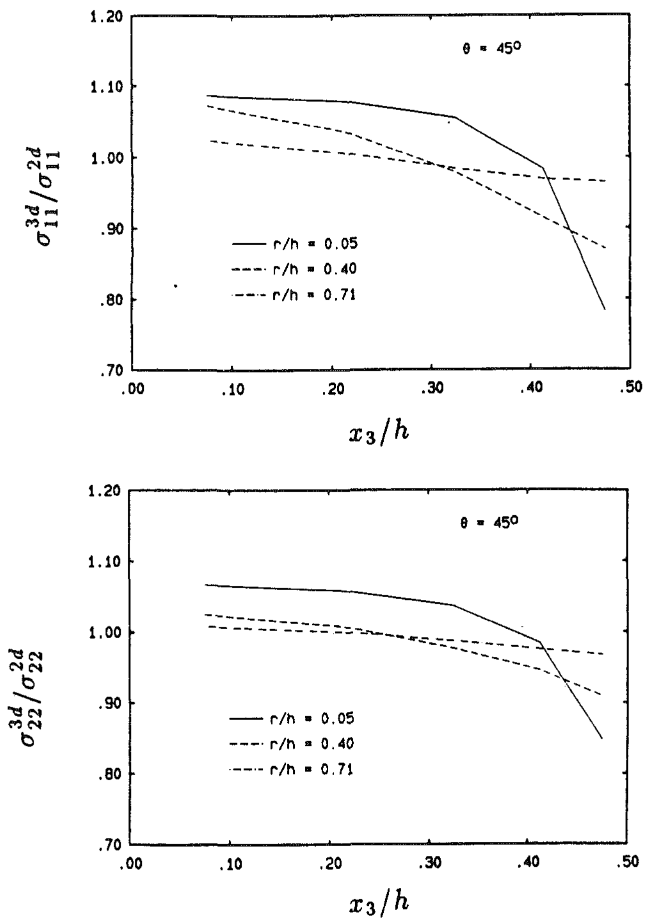

Fig. 13 Representative through thickness variation of normalized stress components

reasons for the observed experimental variation are accounted for by the three-dimensional elastodynamic simulation. Note that it is purely to highlight this point that the above "scaling" procedure was adopted. It is not the intention here to offer Fig. 10(*b*) as some kind of an empirical "correction curve" for experimental data.

Finally, it is instructive to look into some additional features of the near-tip field quantities. Figure 12 shows the near-tip variation of the degree of plane strain for one typical time in the simulation. In regions where plane stress is a good approximation to the actual three-dimensional state of stress, the degree of plane strain must be close to zero. It is seen that, by this measure, plane-stress conditions are obtained at radial distances greater than about one-half plate thickness from the crack front. Also note that the radial extent of the region of three-dimensionality is not uniform around the crack front but varies substantially with angle.

The thickness variations of stress components (σ_{11} and σ_{22} normalized by the corresponding full-field two-dimensional values) are shown for one representative time in Figs. 13(*a*), 13(*b*) for a range of radial distances from the crack tip along the $\theta = 45$ deg line. It can be seen that the deviations in stresses from the two-dimensional fields are largest toward the crack tip and the free surface. Also, these plots underscore the point that the assumption of plane stress is indeed a good one for regions of radial extent greater than about one-half plate thickness away from the crack front. Note, however, that this does not imply that the asymptotic K_I^d-field is dominant in the plane-stress region outside the near-tip zone of three-dimensionality.

4 Discussion

Based on two and three-dimensional elastodynamic simulations of the drop-weight tests, the following conclusions can be drawn:

(i) The dynamic asymptotic field, while sufficiently accurate for $r/h \to 0$, becomes increasingly inadequate for larger radial distances even in a purely two-dimensional setting.

(ii) The three-dimensional nature of the dynamic crack-tip field, which is seen to be confined to within at most one-plate thickness radial extent around the crack-tip, exhibits largest deviation from the full-field plane-stress results for $r/h \to 0$.

(iii) The above two results together imply that the three-dimensional structure of the near-tip surface, coupled with the transient nature of the local fields, appear to preclude any sizeable region of K_I^d-dominance around the crack tip.

The experiments reported in Part I had also indicated the lack of an underlying K_I^d-dominant field. This was observed experimentally for both the dynamically loaded stationary crack as well as for rapidly propagating cracks. While it is recognized that the results of this work are specific to the configuration studied, it is not inconceivable, especially in view of lack of countervailing evidence, that a similar result could hold in other settings. It might thus be instructive to speculate on the validity of the presumed K_I^d-dominance in some of the experiments reported in the literature.

Some Implications of Lack of K_I^d-Dominance. As far as the dominance of a K_I-field is concerned, the ratio of the smallest pertinent in-plane length to the specimen thickness can be thought of as a relevant geometry parameter. As pointed out in Part I, the possible extent of a K_I-dominant annulus around the crack-tip is bounded from within by the maximum extent of (a) the process zone, (b) the nonlinear region, and (c) the three-dimensional region. For nominally brittle materials such as those considered in this work, it appears that three-dimensionality is the most critical of the three. Also, the outer bound for a K_I-dominant annulus around the crack-tip is expected to depend on a relevant in-plane length scale. Thus, under static conditions at least, it is expected that the ratio a/h (where "a" is the smallest relevant in-plane length and "h" is the specimen thickness) must be sufficiently large for a K_I-field to survive the three-dimensional region and establish its dominance over some finite domain. In dynamic problems, the issue is much more involved with additional requirements dictated by the nature of the loading and the time required for stress-wave information to reach regions outside the three-dimensional zone (see, for example, Ravi-Chandar and Knauss, 1987). These, however, would seem to only further restrict the possibility of obtaining a K_I^d-dominant region in a real experiment. Thus, if a/h fails to be sufficiently large, it is not expected that a K_I^d-dominant field would prevail over any finite domain around the crack tip. In particular, note that in the experiments reported in this work, a/h is about 9 (based on the uncracked ligament as the relevant in-plane length) and, for this value, a K_I^d-dominant field was not observed. It might thus be expected that the existence of a K_I^d-dominant region is not assured for specimens for which a/h is of the same order as this work. It is not the authors' intention here to make a detailed review of the experimental literature with a view to ascertaining whether K_I^d-dominance prevailed in these experiments or not. Rather, the parameter a/h is suggested here as one measure by which the interested reader might gauge the relevance of the results of this work to other experiments. In the following, some issues on which the results of this work might have a bearing are briefly discussed.

On K_{ID}—$\dot{a}$ *Relations:* The question of the precise functional dependence of the dynamic fracture toughness on the crack velocity has appropriated a substantial share of the resources devoted to the study of dynamic fracture. The argument, for the most part, has centered around the issue of uniqueness of relationship between K_{ID} and $\dot{a}$. Kobayashi and Dally (1980), Rosakis, Duffy, and Freund (1984), and Zehnder and Rosakis (1989) provide data sets that seem to indicate that the K_{ID}—$\dot{a}$ relation is indeed (to within experimental error) a unique material property. The results of Kobayashi and Mall (1978) and Ravi-Chandar and Knauss (1984)—using photoelasticity and the method of caustics in transmission, respectively—suggest, however, that there is no such one-to-one correspondence. Is the substantial scatter in these data sets due to a lack of a unique correspondence between K_{ID} and $\dot{a}$, or due to a more fundamental lack of a K_I^d-dominant field in the experiments? Also, in all these experiments, the question of whether it is indeed the dynamic stress intensity factor that is being measured needs to be looked into.

On Specimen Dependence of K_{ID}: By far the most troubling of all the experimental results are those that indicate that the dynamic fracture toughness could be specimen dependent (Kalthoff, 1983; Dahlberg, Nilsson, and Brickstad, 1985). These results, rather than merely contending about the parametric dependence of a material property—the fracture toughness—would, if true, seem to indicate that the stress intensity factor based fracture criterion is fundamentally flawed. However, it is possible to attribute the apparent observed specimen dependence of K_{ID} to specimen-dependent differences in the near-tip field (i.e., the near-tip fields, not being K_I^d-dominant, might have a different structure from specimen to specimen). Moreover, as has been shown in this work, much larger differences (than the 20 percent or so that is seen in the results of Kalthoff (1983)) could possibly have been obtained for the *same* type of specimen if, in the caustics experiments used to obtain these results, a different range of initial curves had been used by changing the specimen to image plane distance z_0.

On K_{ID}—$\ddot{a}$ *Relations:* Attempts by Takahashi and Arakawa (1987)—using the method of caustics again—to show acceleration dependence of the dynamic fracture toughness can also be deemed inconclusive for precisely the same reasons as above.

On Photo-elasticity versus Caustics: Nigam and Shukla (1988) have recently tried to compare the methods of photoelasticity and transmission caustics by doing tests on identical specimens under identical loading. They show that while both methods work well for static problems, the method of photoelasticity gives values for the dynamic stress intensity factor which are about 30–50 percent higher than those obtained through the method of caustics. As shown in this paper, this discrepancy could very well be due to violation of K_I^d-dominance assumed in the interpretation of experimental data. Note, in particular, that caustics and photo-elasticity data typically come from different regions around the crack tip.

Finally, the larger question of whether a stress intensity factor based fracture criterion is applicable under conditions of lack of K_I^d-dominance remains to be resolved. By the very nature of its formulation (see Part I), it would seem that a K_I^d-based fracture criterion would be applicable to only that class of problems where there is a K_I^d-dominant region confining the near-tip nonlinear and fracture process zones. Thus, it could be argued that investigations designed to resolve questions of the dependence of the dynamic fracture toughness on crack velocity, acceleration, or specimen geometry, etc., would be meaningful only if (i) the experimental configuration utilized is shown to lead to a region of K_I^d-dominance and (ii) the observed variations are significant in comparison to the uncertainty associated with the assumptions of the experimental techniques used.

5 Conclusion

In this paper, as well as in Part I, an attempt has been made to investigate the consequences of interpreting experimental results using the method of reflected caustics under the assumption of K_I^d-dominance. It was shown that this assumption could lead to substantial errors in the measured results. It is our view that many of the apparent discrepancies in the experimental literature might arise from the lack of an underlying K_I^d-dominant or higher-order two-dimensional region assumed in the interpretation of the experimental data. The assumption that the near-tip region is K_I^d-dominant (or even two-dimensional, for that matter) is only an approximation and, as such, entails a corresponding uncertainty in the measured values for the dynamic stress intensity factor. We feel that it is essential to undertake studies in the spirit of the one reported here to investigate the assumptions of other experimental techniques (photo-elasticity, transmission caustics, etc.) and evaluate the costs incurred in terms of loss of accuracy.

Acknowledgments

The authors would like to thank Prof. M. Ortiz for providing a version of the finite element program, FEAP. Support of the Office of Naval Research through contract N00014-85-K-0599 is gratefully acknowledged. The computations were performed using the facilities of the San Diego Supercomputer Center and were made possible through an NSF-PYI grant MSM-84-51204 to the second author.

References

Bathe, K., 1982, *Finite Element Procedures in Engineering Analysis*, Prentice Hall.

Dahlberg, L., Nilsson, F., and Brickstad, B., 1980, "Influence of Specimen Geometry on Crack Propagation and Arrest Toughness," *Crack Arrest Methodology and Applications*, G. T. Hahn et al., ed., ASTM-STP 711, pp. 89–108.

Dally, J. W., Fourney, W. L., and Irwin, G. R., 1985, "On the Uniqueness of K_{ID}—$\dot{a}$ Relation," *International Journal of Fracture*, Vol. 27, pp. 159–168.

Hinton, E., and Campbell, J. S., 1974, "Local and Global Smoothing of Discontinuous Finite Element Functions Using a Least Squares Method," *International Journal for Numerical Methods in Engineering*, Vol. 8, pp. 461–480.

Hughes, T. J. R., and Belytschko, T., 1983, "A Precis of Developments in Computational Methods for Transient Analysis," ASME Journal of Applied Mechanics, Vol. 50, pp. 1033–1041.

Kalthoff, J. F., 1983, "On Some Current Problems in Experimental Fracture Mechanics," *Workshop on Dynamic Fracture*, W. G. Knauss et al., ed., California Institute of Technology, pp. 11–35.

Kobayashi, A. S., and Mall, S., 1978, "Dynamic Fracture Toughness of Homalite 100," *Experimental Mechanics*, Vol. 18, pp. 11–18.

Kobayashi, T., and Dally, J. W., 1980, "Dynamic Photo-elastic Determination of the $\dot{a}$—K Relation for the 4340 Steel," *Crack Arrest Methodology*, G. T. Hahn et al., ed., ASTM-STP 711, pp. 89–108.

Krishnaswamy, S., 1988, "On the Domain of Dominance of the Asymptotic Elastodynamic Crack-Tip Fields," doctoral dissertation, California Institute of Technology, Pasadena.

Levy, N., Marcal, P. V., and Rice, J. R., 1971, "Progress in Three-Dimensional Elastic Stress Analysis for Fracture Mechanics," *Nuclear Engineering and Design*, Vol. 17, pp. 64–75.

Nakamura, T., and Parks, D. M., 1987, "Three-Dimensional Field Near the Crack Front of a Thin Elastic Plate," presented at the 24th Annual Meeting of the Society of Engineering Science, Sept. 21–23, 1987, Salt Lake City, Utah.

Nakamura, T., and Parks, D. M., 1988, "Conditions for J-Dominance in Three-Dimensional Thin Cracked Plates," *Analytical, Numerical and Experimental Aspects of Three-Dimensional Fracture Process*, A. J. Rosakis et al., ed., ASME-AMD, Vol. 91, pp. 227–238.

Nakamura, T., Shih, C. F., and Freund, L. B., 1986, "Three-Dimensional Transient Analysis of a Dynamically Loaded Three-Point Bend Ductile Fracture Specimen," Brown University Report, ONR 0365/13, Brown University.

Narasimhan, R., and Rosakis, A. J, 1988, "Three-Dimensional Effects Near a Crack-Tip in a Ductile Three-Point Bend Specimen; Part I: A Numerical Investigation," SM-Report 88-6, GALCIT, California Institute of Technology.

Nigam, H., and Shukla, A., 1988, "Comparison of the Techniques of Transmitted Caustics and Photoelasticity as Applied to Fracture," *Experimental Mechanics*, Vol. 28, No. 2, pp. 123–133.

Parsons, I. D., Hall, J. F., and Rosakis, A. J., 1986, "A Finite Element Investigation of the Elastostatic State Near a Three-Dimensional Edge Crack," GALCIT Report SM 86-29, California Institute of Technology.

Ravi-Chandar, K., and Knauss, W. G., 1984, *International Journal of Fracture*, Vol. 25, pp. 247–262.

Ravi-Chandar, K., and Knauss, W. G., 1987, "On the Characterization of the Transient Stress Field Near the Tip of a Crack," ASME Journal of Applied Mechanics, Vol. 54, pp. 72–78.

Rosakis, A. J., and Freund, L. B., 1981, "The Effect of Crack-Tip Plasticity on the Determination of the Dynamic Stress-Intensity Factor by the Optical Method of Caustics," ASME Journal of Applied Mechanics, Vol. 48, pp. 302–308.

Rosakis, A. J., Duffy, J., and Freund, L. B., 1984, "The Determination of Dynamic Fracture Toughness of AISI 4340 Steel by the Shadow Spot Method," *Journal of the Mechanics and Physics of Solids*, Vol. 32, pp. 443–460.

Smith, R. H., and Freund, L. B., 1988, "Three-Dimensional Finite Element Analysis of Steady Elastodynamic Crack Growth in a Plate," presented at the joint ASME-SES Conference, June 1988, Berkeley, Calif.

Takahashi, K., and Arakawa, K., 1987, "Dependence of Crack Acceleration on the Dynamic Stress-Intensity Factor in Polymers," *Experimental Mechanics*, Vol. 27, No. 2, pp. 195–199.

Taylor, R. L., 1977, "Computer Procedures for Finite Element Analysis," *The Finite Element Method*, 3rd ed., by O. C. Zienkiwiecz, McGraw-Hill, New York.

Zehnder, A. T., and Rosakis, A. J., 1989, "Dynamic Fracture Initiation and Propagation in 4340 Steel Under Impact Loading," *International Journal of Fracture*, to appear.